Open Ceramics 20 (2024) 100707

Contents lists available at ScienceDirect

Open Ceramics

journal homepage: www.sciencedirect.com/journal/open-ceramics

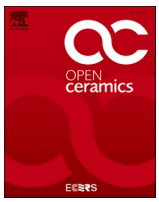

Using percolation to design ZnO composites with hBN modified grain boundaries to obtain varistor-like behavior

Michael W. Mervosh [a,b,*], Sevag Momjian [a,b], Javier Mena-Garcia [a,b], Clive A. Randall [a,b]

[a] Department of Materials Science and Engineering, The Pennsylvania State University, University Park, PA, 16802, USA
[b] Materials Research Institute, Millenium Science Complex, University Park, PA, 16802, USA

ARTICLE INFO

Keywords:
Varistor
Cold sintering
Percolation
Boron nitride

ABSTRACT

Conventional varistors rely on the formation of a Double Schottky Barrier within the intergranular region of ZnO via acceptor doping and a Bi_2O_3 phase. This work has been able to yield varistor-like behavior via cold sintered ZnO composites by placing 2D hBN flakes on the grain boundaries within the ZnO matrix. Above the percolation threshold, a network of resistive hBN barriers is formed which prevents current from flowing through the more conductive ZnO. However, at a given voltage, electrons can tunnel through the hBN if the layers are kept thin enough. Within this narrow band of hBN content, samples have been fabricated with α values as high as 9.5. The composite system demonstrated Schottky conduction at low fields before switching to Fowler-Nordheim tunneling at high fields. This microstructural design was able to show greater nonlinearity compared to previous attempts at creating varistor materials through the unique cold sintering process (CSP).

1. Introduction

Varistors are voltage dependent resistors that possess high resistivity at low applied voltages before switching to a lower resistivity at higher voltages. Thus, varistors obey Ohm's law (V = IR) at low voltages before switching to a non-Ohmic behavior defined by the following expression [1]:

$$I = KV^{\alpha} \tag{1.1}$$

Above, I is current, K is a proportionality constant, V is voltage, and α is the nonlinear coefficient. An $\alpha \approx 1$ indicates Ohmic linear behavior while an α above 1 indicates varistor-like behavior. This variable response to voltage provides the functionality that is useful for protecting vulnerable circuits from power surges and voltage spikes that would otherwise destroy sensitive components [1–3]. Most of the varistors manufactured today are made of ZnO, SiC, or $SrTiO_3$ and rely on electrostatic potential barriers to generate a voltage dependent resistivity [2]. These special grain boundaries are known as double Schottky barriers (DSB) and typically use a doped Bi_2O_3 intergranular phase at the grain boundaries of the ZnO matrix [3,4]. ZnO acts as an n-type semiconductor, meaning it has excess electrons that aid in its conductivity. In the case of varistors, acceptor states are added to the grain boundaries and these states trap electrons from the bulk. This leads to a depletion of charge carriers at the grain boundaries and an accumulation of holes (positively charged states). The flow of electrons is thus opposed by the internal field formed at the boundary between 2 grains [5]. In order to introduce these acceptor states into the intergranular layer (IGL), dopants are added by sintering ZnO in a liquid phase. This will allow the ions in the solution to surround the ZnO grains and diffuse into the surfaces creating electronic traps at the interfaces.

The Cold Sintering Process (CSP) has been investigated in the past to serve as a more sustainable ceramic manufacturing process [6]. CSP densifies samples at temperatures below 350°C with the aid of pressures on the order of hundreds of MPa. This is done in the presence of a transient phase which drives a pressure-solution creep (PSC) process to transport material during densification [7,8]. Typically, this liquid phase is an organic acid capable of dissolving and transporting the bulk material to drive PSC [9]. Under an applied load, the liquid partially dissolves the powder and transfers the solute along the grain boundaries of the matrix. The powder is then redeposited at the pores driven by chemical potential gradients. Thus, the pores are slowly filled in with time and samples are able to be densified to above 95% relative density [10]. The low temperatures involved allow for the fabrication of novel materials that would otherwise degrade or form unwanted secondary phases with conventional sintering [11,12,13]. This novel manufacturing process has been used in the past to design varistor

* Corresponding author at: N-244, Millennium Science Complex, University Park, PA, 16802, USA
E-mail address: mwm6270@psu.edu (M.W. Mervosh).

https://doi.org/10.1016/j.oceram.2024.100707
Received 28 August 2024; Received in revised form 30 October 2024; Accepted 12 November 2024
Available online 14 November 2024

components incorporating polymer filler at the grain boundaries of ZnO [2,10].

CSP has also been used to fabricate hexagonal boron nitride-containing composites to boost the electrical resistivity of a given system while simultaneously increasing thermal conductivity [10,14]. Hexagonal boron nitride (hBN) is a 2D material with a crystal structure closely related to that of graphite. It is for this reason that hBN is often referred to as "white graphite" which also gives a nod to the material's pale color [15]. The bonding within layers is covalent while the bonding between layers arises due to Van der Waals forces. This leads to a high degree of anisotropy in hBN's properties and allows for these hBN sheets to be easily pulled apart from one another as the bonds between the planes are much weaker than those in plane [16]. Mechanical shearing is what makes 2D materials like hBN perfect candidates for demonstrating percolation theory. Under an applied stress, the hBN particles are cleaved and readily slide around the matrix grains. Given that hBN gains no free electrons nor ions from its bond type, it has exceptionally high electrical resistivity. This value has been reported as high as 10^{15} Ωcm placing it among the most electrically insulating materials in use today [16]. It thus follows that hBN also has a high dielectric breakdown strength (E_b), though it does exhibit an anisotropic response. In plane, its E_b value is 3MV/cm and out of plane this number jumps to 12MV/cm [16]. A recent study by Mena et. al utilized the high thermal conductivity (κ) of hBN in a $Na_2Mo_2O_7$ microwave dielectric to improve the electrical and thermal properties of the system [14]. Building from these observations, the highly resistive nature of hBN along with its capacity to easily shear and percolate through a matrix were the main reasons for choosing this material in a composite ZnO varistor system.

The goal of this study was to employ CSP to create ZnO – hBN composites and assess their varistor capabilities. It was surmised that the hBN would shear and form a resistive network around the ZnO grains to block electron flow at low voltages providing a varistor response in a unique microstructural design.

2. Experimental procedure

2.1. Cold sintering procedure

In order to coarsen the ZnO powder to allow for more efficient shearing of the hBN particles, the ZnO (40 – 100nm Alfa Aesar, Haverhill, MA) was annealed at 900°C for 5 hours. This generated ZnO grains with a particle size of 3.2 ± 1.0μm. It should be noted that smaller particle sizes (200nm) of ZnO have been cold sintered in the past but for this study such powders were unable to effectively disperse the hBN flakes [2,6]. A comparison of the degree of hBN shearing between the fine and coarse ZnO powders can be found in Supplemental Information Fig. S1. Next, the proper amounts of ZnO and hBN (99.8%, 70–80 nm, Nanoshel, Wilmington, DE) powder were weighed out to fabricate cold sintered composite pellets. These composites contained 0, 2.5, 4.0, 6.0, 10.0, 20.0, 30.0, and 40.0 volume % hBN. The weighed powders were placed in a glass vial and mixed under dry conditions using a planetary centrifugal mixer (ARE-250, Thinky, Tokyo, Japan) for 10 cycles of 1 minute each. Then, 15 weight % of 2M acetic acid was added to the powder and the materials were mixed in an agate mortar with a pestle until a homogeneous mixture was obtained. The "wet" powder was placed in a steel die (13mm in diameter) separated from the pucks of the die by disks of Ni foil. It should be noted that the mixture easily flows into the die and the liquid content is so low that it does not reflect a colloid but rather a powder. The die was placed under a uniaxial pressure of 300 MPa and heated to 150°C for 4 hours at 20°C/min using a heating jacket controlled by a Proportional–Integral–Derivative loop feedback mechanism. A thermocouple was placed in a slit at the bottom of the die base. After the 4 hours had elapsed, the 1.3mm thick pellet was ejected from the die and allowed to cool to room temperature. Finally, the pellets were polished on the faces and edges using methanol propylene glycol (Allied High Tech Products, Compton, CA) and SiC paper (to 1200 grit). A full schematic of this process is given in Fig. 1. The ZnO samples yielded relative density values of 92.2 ± 2% based on the theoretical densities of the samples' respective compositions. A more detailed breakdown of sample densities is shown in Fig. 2.

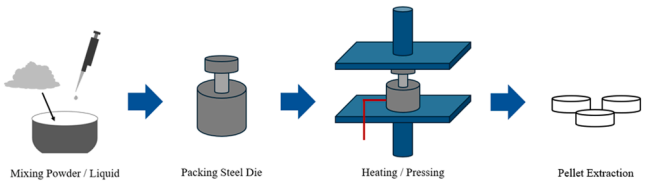

Fig. 1. Diagram of complete cold sintering process.

2.2. Material characterization

To equip the samples with conductive electrodes for all subsequent electrical measurements, the pellets were first coated with 100nm of platinum on both sides. The coatings were sputtered under an Ar atmosphere using a physical vapor deposition chamber (Q150V, Quorum Technologies, Lewes, UK). To test for resistivity, the coated samples were subjected to a voltage of 1V which was held for 4 minutes to allow for current stabilization. This was done using a Hewlett-Packard 4140B pA Meter / DC Voltage Source.

Using the same system as the resistivity measurements, I-V measurements were performed on the ZnO composites with varying volume fractions of hBN. Given the high voltages employed, the amplifier adapter for this setup was activated. The measurements started with an applied voltage of 10V and increased up to 1,000V in increments of 10V. Both the applied voltages and their corresponding measured currents across the sample were reported and used to construct IV curves for the various samples. For calculating Schottky barriers, these samples also had their IV behavior measured between 1V and 20V at 20°C, 40°C, 60°C, and 80°C. This same characterization system was used to extract data necessary for the Fowler-Nordheim plots. The samples were subjected to a voltage range beginning at 10 V and ending at the breakdown voltage of the material. This was carried out at 40°C, 60°C, 80°C, and 100°C.

The microstructures of the ZnO composites were analyzed by Scanning Electron Microscopy (SEM) employing a Field Emission Scanning Electron Microscope (Verios, Thermo Fischer Scientific, Waltham, MA). To avoid significant charging on the surface of the samples, each sample was coated with 5nm of iridium in a physical vapor deposition chamber (EM ACE200, Leica, Wetzlar, Germany). The interfaces observed were also analyzed using Energy Dispersive Spectroscopy (EDS) to map the composition of the material.

3. Results and discussion

3.1. Microstructure analysis

Based on an earlier work involving $Na_2Mo_2O_7$ - hBN composites, it was suspected that the microstructure for this system would feature sheared hBN on the grain boundaries of the matrix material [14]. This was confirmed by the SEM images shown in Fig. 3A and B. One can see the hBN flakes encompassing the ZnO grains after being sheared by said

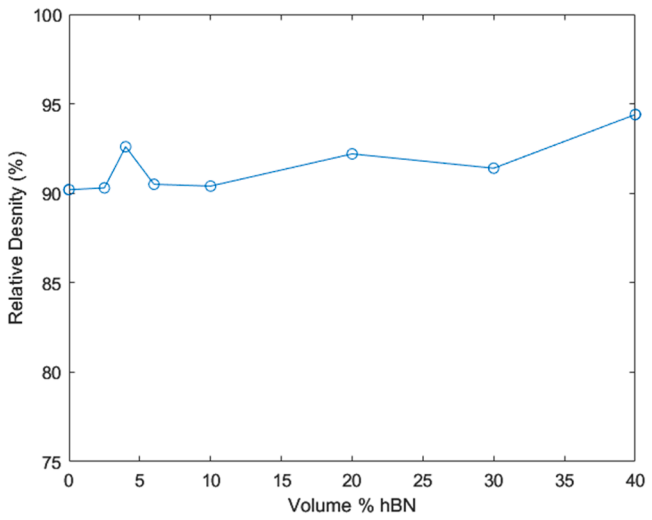

Fig. 2. Relative densities of ZnO composites containing between 0 – 40 vol % hBN.

grains under the applied load. This shearing was possible due to the layered structure of hBN which contains weak, easily broken Van der Waals forces between planes [17]. The behavior of 2D materials when subjected to CSP has been widely studied in the past in the cases of graphite, hBN, WS_2, MoS_2, and SnS_2 [18,19]. These materials are prone to plastic deformation and slip under applied loads large enough to eclipse their critical shear strains. The slip mechanism at play here was described as a "deck of cards" by Soule and Nezbeda with layers successively shearing and slipping below one another [20]. It is for this reason that at high pressures, one sees the hBN deform and fill in the sample's pores as the original flakes are fanned out [18,20].

The evolution of the microstructure for these composites as a function of hBN content can be seen in Fig. 3C–F. The sample below the percolation threshold in Fig. 3D shows minimal signs of hBN with some flakes appearing within the pores and between the ZnO grains. Then, above the threshold at 4 vol% one sees the hBN has been sheared around the ZnO grains and exists in thin layers at the grain boundaries. Lastly, Fig. 3F shows a sample well above the percolation threshold where hBN particles continue to surround the ZnO but the layers are now much thicker at the grain boundaries.

Looking closer at the microstructure observed in a sample containing 4 vol% hBN, one can see that there is a degree of heterogeneity in the thickness of the hBN. Fig. 4 shows that as the hBN sheets are sheared/spread out along the ZnO grains, some regions are multiple layers thick while others (shown by the red circles) are 1 or 2 layers thick. It is believed that these thinner regions act as the tunneling points that will be described in subsequent sections. Thus, it follows that increasing hBN content far above the percolation threshold would decrease the prevalence of these thin tunneling regions.

3.2. Resistivity results

It was believed that an optimal varistor response from this system would be found at a volume fraction of hBN close to the percolation

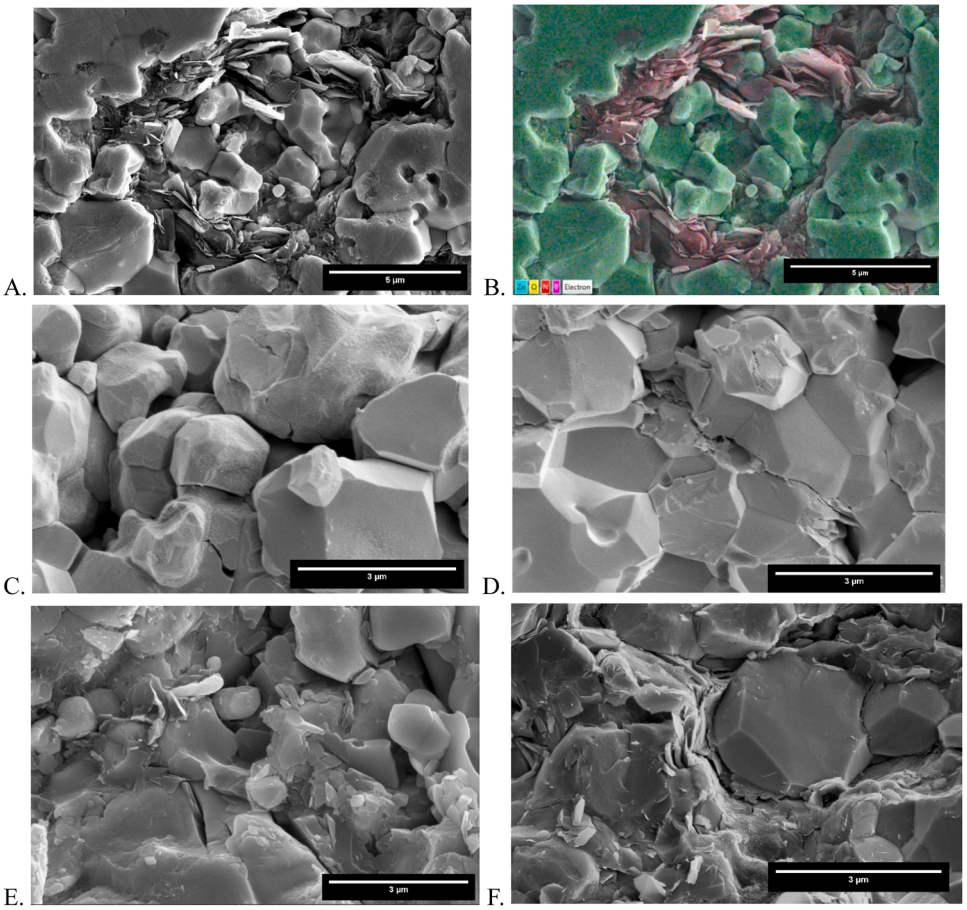

Fig. 3. (A) SEM image of ZnO with 20 vol% hBN (B) EDS mapping of same ZnO – 20 vol% hBN sample showing hBN flakes (red/pink) surrounding ZnO grains (blue/yellow) (C) SEM image of pure ZnO (D) SEM image of ZnO - 2.5 vol% hBN (E) SEM image of ZnO - 4 vol% hBN (F) SEM image of ZnO - 10 vol% hBN. (For interpretation of the references to color in this figure legend, the reader is referred to the web version of this article.)

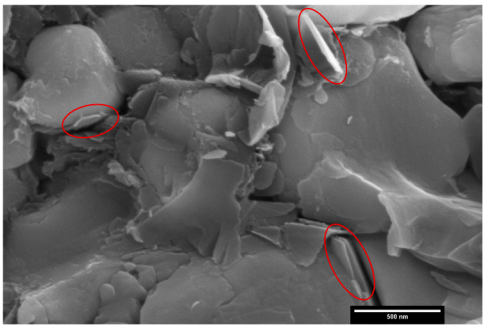

Fig. 4. Heterogeneities in hBN thickness in a ZnO – 4 vol% hBN sample indicating 1-to-2-layer thick hBN sheets with red circles.

threshold. Such samples would have sufficient encapsulation of the ZnO grains to block any conductive paths within the matrix. However, the hBN content would still be low enough to preserve the thinner pockets of hBN described in Fig. 4. The thickness of the layers is crucial as the hBN must be thin enough to still allow for electron tunneling at high voltages. For instance, previous studies investigating Fowler Nordheim tunneling in hBN found that the hBN layers must be less than 10nm thick [21].

To determine the percolation threshold of the ZnO – hBN system, the resistivity as a function of vol% hBN plot in Fig. 5 was crafted. The data was fitted to a curve using two equations from percolation theory [22]. The first equation is shown below and applies to reported resistivity values when one is below the percolation threshold:

$$\rho = \rho_m \left(\frac{\varphi_c - \varphi_f}{\varphi_c} \right)^{-s} \tag{3.1}$$

In the above equation, ρ is the resistivity of the resultant composite, ρ_m is the resistivity of the matrix, φ_f is the volume fraction of the filler, φ_c is the percolation threshold, and s is a critical exponent. For volume fractions above the percolation threshold, the following equation was used:

$$\rho = \rho_f (\varphi_f - \varphi_c)^t \tag{3.2}$$

In the above equation, ρ is the resistivity of the resultant composite, ρ_f is the resistivity of the filler, φ_f is the volume fraction of the filler, φ_c is the percolation threshold, and t is a critical exponent. Using this

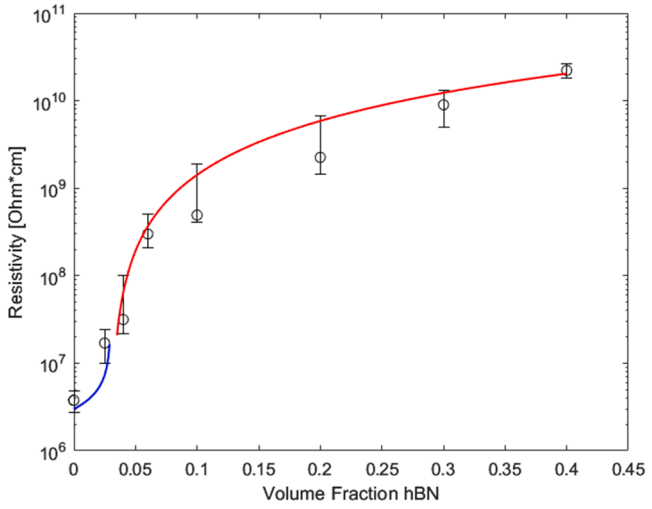

Fig. 5. Percolation curve for ZnO composites. The blue line is fitted to Eq. 3.1 below the percolation threshold, the red line is fitted to Eq. 3.2 above the threshold. (For interpretation of the references to color in this figure legend, the reader is referred to the web version of this article.)

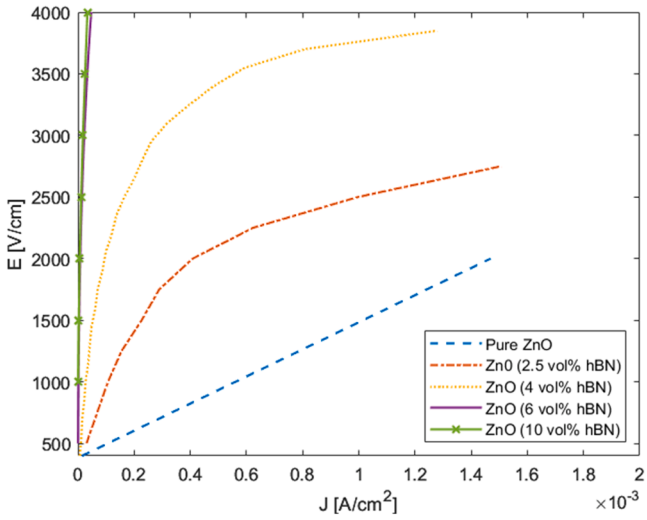

Fig. 6. Electric field vs. current density for ZnO composites.

derivation technique, s was 0.5, t was 1.6, and the percolation threshold was found to be 3 vol% to satisfy Eqs. 3.1 and 3.2 .

3.3. Current voltage (IV) analysis

The results of the IV curve measurements are shown in Fig. 6 and expressed in terms of the electric field E vs. current density J with the slope indicating resistivity. As expected, the pure ZnO shows a linear trend with respect to electric field vs. current density. The samples with volume fractions of hBN close to the percolation threshold then demonstrate a non-linear trend. Once the percolation region for this system is eclipsed, IV behavior then returns to linearity with a significantly steeper slope than pure ZnO indicating higher resistivity. These results validate the hypothesized system at work in ZnO – hBN composites. Thin enough layers of hBN on the grain boundaries oppose conductivity up to a voltage limit before there exists sufficient energy to tunnel through the hBN layers at the thinnest points. Even a hBN content of 6% proves to be too high and causes the system to remain resistive across the measured voltages. There exists a narrow region capping the percolation threshold on either side that yields varistor – like behavior in these composite samples.

To quantify the non-linear trend of these varistors, the α values for these composites were calculated. These values were obtained by taking the slope of a log(V) vs. log(I) plot in the region between 0.1 and 1.0mA. The magnitude of α is equal to the inverse of the slope in this region [3]. The log(V) vs. log(I) plot used for this study can be found in Fig. S2. Table 1 shows the reported α values for each tested sample. The values peak around the percolation threshold then decrease to a more linear indication above and below these values. Previous studies using ZnO – polymer varistors engineered by CSP have reported values between 4 and 7 [2,6]. The samples in this study reported a peak α value of 9.51 corresponding to a hBN content of 4 vol %. This demonstrates the validity of this 2D filler based approach to achieve non-linearity while

Table 1
Calculated α values and breakdown voltages for ZnO composites.

Sample:	α value:	$E_{0.1mA}$ (V/cm)	$E_{0.1mA}$ (V/gb)
Pure ZnO	1.77	1500	0.48
ZnO (2.5% hBN)	6.00	2500	0.80
ZnO (4.0% hBN)	9.51	3700	1.2
ZnO (6.0% hBN)	2.85	6200	2.0
ZnO (10% hBN)	2.32	7000	2.2

improving upon previous attempts to use CSP composites in varistor applications. The breakdown field values at 0.1 mA are also found in Table 1 reported alongside the corresponding voltage per grain boundary values (the derivations of which can be found in Supplemental Information). As expected, the breakdown voltages increase with hBN content as the grain boundary region becomes more resistive with thicker hBN. It is worth noting that these breakdown field values are an order of magnitude smaller than those reported in other ZnO varistor studies using CSP [2,6]. This can be explained by the larger grain sizes that had to be employed by this study to facilitate the shearing of the hBN particles. The breakdown voltage per grain boundary values report magnitudes more in tune with those found in the literature for conventional varistors with DSBs at the grain boundaries. Although, the optimal 4 vol% hBN sample is still slightly below typical breakdown voltage values which may be explained by a thinner depletion layer since no holes have been engineered into the IGL.

3.4. Fowler Nordheim analysis

To showcase the transition from Schottky controlled to tunneling controlled conduction in this system, a Fowler-Nordheim plot was constructed for a sample containing 4 vol% hBN. The plot in Fig. 7 shows a linear response for all probing temperatures at high applied electric fields. The system no longer relies solely on thermionic emission for electrons to transverse the IGL and tunneling becomes the dominant conduction mechanism at these higher fields. Once the electric field is reduced, the system switches back to Schottky conduction where there is a clear dependence on temperature. The temperature independent regime is shown by the green line and follows the given equation [10]:

$$J = AE^2 \exp\left(\frac{\gamma}{E}\right) \tag{3.3}$$

Above, J is current density, A and γ are both constants, and E is the applied electric field. In the case of the ZnO - 4 vol% hBN sample, A was found to be 3.0×10^{-12} and γ was found to be 2,000 V/cm. Using these values, it is also possible to calculate the barrier height of Fowler-Nordheim tunneling using the following equation [10]:

$$\gamma = \frac{8\pi\sqrt{2m^*}}{3qh}(q\Phi)^{3/2} \tag{3.4}$$

Above, m^* is effective mass (which for ZnO is $0.23m_o$ [23]), q is charge of an electron, h is Planck's constant, and $q\Phi$ is barrier height. In the case of the ZnO - 4 vol% sample, its barrier height was found to be 0.15 eV which is comparable to the 0.1 eV reported for the cold sintered ZnO – TrFE (Trifluoroethylene) system studied by Mena-Garcia et. al

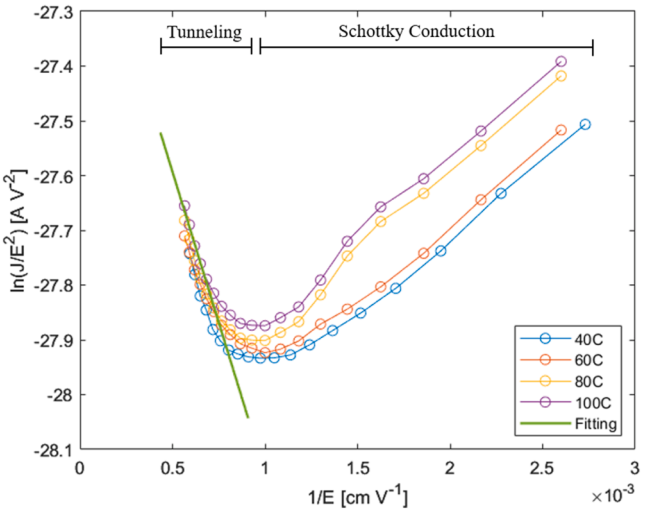

Fig. 7. Fowler – Nordheim diagram of ZnO - 4 vol% hBN.

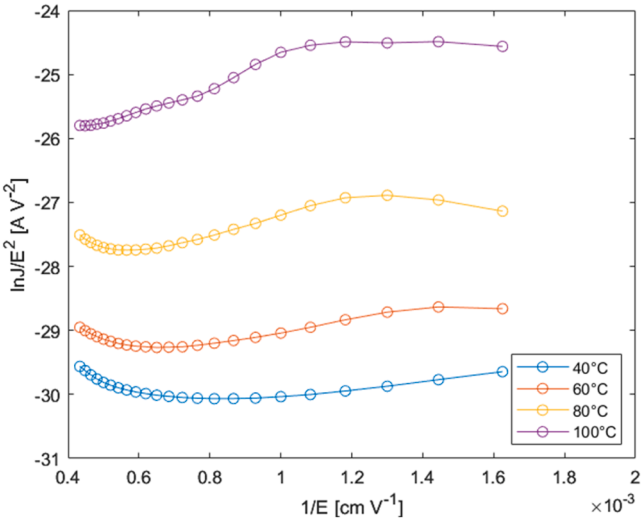

Fig. 8. Fowler – Nordheim diagram of ZnO - 10 vol% hBN.

[10] .

The above Fowler – Nordheim diagram is contrasted by the results of a sample with a volume fraction of hBN well above the percolation threshold. Fig. 8 shows a Fowler – Nordheim diagram for a sample containing 10 vol% hBN. The system never switches to Fowler – Nordheim conduction and maintains a strong temperature dependence across all measured voltages. This is to be expected given the thicker hBN layers that would be present on the ZnO grain boundaries for this system. It was previously stated that in order for electrons to tunnel under this method, the thickness of the tunneling medium must be less than 10nm. This is not attained with 10 vol% hBN, and thus no two-stage mechanism is present with only Schottky conduction observed in this sample.

3.5. Quantitative Schottky barrier height

To track changes in barrier formation as a function of hBN content at low voltages, Schottky barrier heights were calculated for ZnO composites containing between 0 and 10 vol% hBN. These values were obtained using the equation shown below [24]:

$$J = A^* T^2 \exp\left(-\frac{\Phi}{kT}\right)\left(\exp\left(\frac{qU}{nkT}\right) - 1\right) \tag{3.5}$$

Above, J is current density, A^* is the Richardson constant, T is temperature, Φ is the Schottky barrier height, k is Boltzmann's constant, n is the ideality factor, U is applied voltage, and q is the charge of an electron. Fig. 9 shows the resultant plots derived for pure ZnO to serve as an example of the calculation techniques employed to extract these parameters. Using the Schottky barrier height data, graphs were crafted plotting $\ln(J / T^2)$ vs. $E^{1/2}$ such as the one in Fig. 9A. One then selects an $E^{1/2}$ value where all 4 temperature trends are linear and possess the same slope. The currents corresponding to this $E^{1/2}$ are used to plot $\ln(J / T^2)$ vs. $1/T$ as shown in Fig. 9B. From this plot, one can extract the Richardson constant for this system since the y-intercept of the crafted line is equal to $\ln(A^*)$. Finally, one returns to the original plot whose y-intercept is equal to $\ln(A^*) - \Phi/KT$ and the barrier height is found with simple algebra.

The calculated Schottky barrier heights can be found in Table 2. The pure ZnO sample yielded a Schottky barrier height (Φ) of 0.22eV while the ZnO - 4 vol% hBN sample yielded a barrier height of 0.51eV. A Schottky barrier height of 0.51 eV is slightly higher than the 0.33 eV reported in a study by Zhao et al. investigating ZnO – PTFE variators enabled by CSP [2]. This again shows the change in behavior that was expected from these composites. The barrier height is increased upon

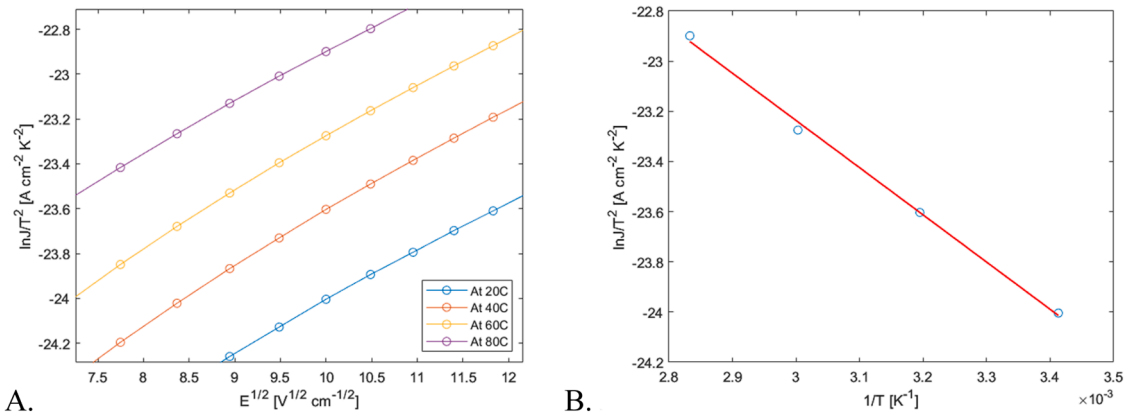

Fig. 9. Plots for deriving Schottky barrier height of pure ZnO.

Table 2
Schottky barrier heights of composites samples.

Sample:	Schottky Barrier Height (eV):
Pure ZnO	0.22
ZnO (2.5% hBN)	0.39
ZnO (4.0% hBN)	0.51
ZnO (6.0% hBN)	1.0
ZnO (10% hBN)	1.6

the inclusion of hBN, meaning more energy is required to allow for electrons to travel between ZnO grains. This increase in required energy hints towards the thickening of the hBN layers as vol% hBN increases. At low applied fields, this energy is supplied via thermionic emission and the electrons follow Schottky conduction [25]. The nearly linear increase in Schottky barrier height with hBN content is to be expected given the microstructure of this system. While the resistivity will follow a percolation trend with a considerable jump following the threshold of 3 vol%, the system possesses some thinner sections of hBN. Thus, with a temperature dependent conduction mechanism like thermionic emission, electrons would begin to conduct through the thinnest sections of hBN aided by heat. The fact that the α values for the 6 and 10 vol% samples are above 1 demonstrates that these thinner hBN sections must still exist to some degree in these samples (though certainly not to the extent of the 4 vol% case). So, their barrier heights will not increase as dramatically as room temperature resistivity given that their dependence on the presence of hBN goes beyond mere encapsulation [26]. It is also important to note that the barrier height to conduction for the 4 vol % hBN is lower for Fowler-Nordheim compared to Schottky conduction. Thus, it follows that the material becomes more conductive once Fowler-Nordheim tunneling is activated at high voltages, leading to the variable resistor response observed for this composite.

4. Conclusions

Composites with a ZnO matrix containing between 2.5 and 40 vol% hBN filler have been fabricated through the cold sintering process with relative densities exceeding 92%. These samples were tested for their IV response and demonstrated varistor behavior in a narrow band of hBN content. The system followed Ohm's Law in pure ZnO before changing to a non-linear response near the percolation threshold of 3 vol% and then switching back to linear above 6 vol%. This change in varistor behavior can be explained by hBN thickness on the ZnO grain boundaries. Once the percolation threshold of 3 vol% hBN has been reached, a resistive network has encapsulated the ZnO grains blocking any conductive paths at low voltages. Then, at high voltages electrons can tunnel through the hBN layers and boost the conductivity of the system so long as the hBN layers are kept thin enough. If one increases hBN content further beyond the threshold, the hBN is too thick to allow for electron tunneling and the system remains resistive at high voltages. This impact on conductivity due to layer thickness was evident in the breakdown voltages and Schottky barrier heights of the samples which increased systematically with volume fraction of hBN. The optimal hBN content was found to be 4 vol% which exhibited a peak α value of 9.51. Through Fowler-Nordheim analysis, it was shown that the optimal varistor specimen followed Schottky conduction at low voltages and Fowler-Nordheim tunneling at high voltages. Such a shift in conduction mechanisms was not observed in a sample containing 10 vol% hBN given the high hBN content. This work has improved upon previous attempts to design a varistor using CSP and demonstrated a novel approach to varistor formation based on percolation in composites.

CRediT authorship contribution statement

Michael W. Mervosh: Writing – original draft, Project administration, Methodology, Investigation, Formal analysis, Data curation, Conceptualization. **Sevag Momjian:** Writing – review & editing, Formal analysis, Data curation, Conceptualization. **Javier Mena-Garcia:** Writing – review & editing, Data curation. **Clive A. Randall:** Writing – review & editing, Supervision, Project administration, Investigation, Funding acquisition, Conceptualization.

Declarations of competing interest

The authors declare that they have no known competing financial interests or personal relationships that could have appeared to influence the work reported in this paper.

Acknowledgements

This material is based upon work supported by the National Science Foundation, as part of the Center for Dielectrics and Piezoelectrics under Grant Nos. IIP-1361571 and IIP-1361503. We would like to thank the staff at the Materials Characterization Lab at Penn State University for their assistance with equipment operation. We also thank the industry partners who support our work and offer assistance when possible.

Supplementary materials

Supplementary material associated with this article can be found, in the online version, at doi:10.1016/j.oceram.2024.100707.

References

[1] Sumit. Vyas, A short review on properties and applications of zinc oxide based thin films and devices, Johnson Matthey Technol. Rev. 64 (2) (2020) 202–218, https://doi.org/10.1595/205651320X15694993568524.

[2] Xuetong Zhao, et al., Introducing a zno–PTFE (polymer) nanocomposite varistor via the cold sintering process, Adv. Eng. Mater. 20 (7) (2018), https://doi.org/10.1002/adem.201700902. .

[3] Mohammad. Reza, Metal oxide ZnO-based varistor ceramics, Adv. Ceram. - Electric Magn. Ceram. Bioceram. Ceram. Environ. (2011), https://doi.org/10.5772/23601.

[4] David R. Clarke, Varistor ceramics, J. Am. Ceram. Soc. 82 (3) (1999) 485–502, https://doi.org/10.1111/j.1151-2916.1999.tb01793.x.

[5] Jinliang He, et al., Electrical degradation of double-Schottky barrier in ZnO varistors, AIP Adv. 6 (3) (2016), https://doi.org/10.1063/1.4944485.

[6] Anna Galotta, Vincenzo M. Sglavo, The cold sintering process: a review on processing features, densification mechanisms and perspectives, J. Eur. Ceram. Soc. 41 (16) (2021) 1–17, https://doi.org/10.1016/j.jeurceramsoc.2021.09.024.

[7] Jing Guo, et al., Cold sintering: progress, challenges, and future opportunities, Annu Rev. Mater. Res. 49 (1) (2019) 275–295, https://doi.org/10.1146/annurev-matsci-070218-010041.

[8] Jing Guo, Amanda L. Baker, et al., Cold sintering process: a new era for ceramic packaging and microwave device development, J. Am. Ceram. Soc. 100 (2) (2016) 669–677, https://doi.org/10.1111/jace.14603.

[9] Sun Hwi Bang, et al., Mechanistic approach to identify densification kinetics and mechanisms of zinc oxide cold sintering, SSRN Electron. J. (2019), https://doi.org/10.2139/ssrn.3428070.

[10] Javier Mena-Garcia, et al., Integration and characterization of a ferroelectric polymer PVDF TRFE into the grain boundary structure of zno via Cold Sintering, J. Eur. Ceram. Soc. 42 (6) (2022) 2789–2797, https://doi.org/10.1016/j.jeurceramsoc.2022.01.064.

[11] Sinan Dursun, et al., A route towards fabrication of functional ceramic/polymer nanocomposite devices using the Cold Sintering Process, ACS Appl. Electron. Mater. 2 (7) (2020) 1917–1924, https://doi.org/10.1021/acsaelm.0c00225.

[12] Sibi N, et al., Garnet mineral based composites through cold sintering process: microstructure and dielectric properties, J. Eur. Ceram. Soc. 40 (2) (2020) 371–375, https://doi.org/10.1016/j.jeurceramsoc.2019.09.012.

[13] Jing Guo, Seth S. Berbano, et al., Cold Sintering process of composites: bridging the processing temperature gap of ceramic and Polymer Materials, Adv. Funct. Mater. 26 (39) (2016) 7115–7121, https://doi.org/10.1002/adfm.201602489.

[14] Javier Mena-Garcia, et al., Dielectric, electrical and thermal properties of sodium molybdate-hexagonal boron nitride composites enabled by cold sintering, Ceram. Int. (2024), https://doi.org/10.1016/j.ceramint.2024.05.155.

[15] S. Majety, et al., Semiconducting hexagonal boron nitride for deep ultraviolet photonics, in: Quantum Sensing and Nanophotonic Devices IX, 2012, https://doi.org/10.1117/12.914084.

[16] Soumyabrata Roy, et al., Structure, properties and applications of two-dimensional hexagonal boron nitride, Adv. Mater. 33 (44) (2021), https://doi.org/10.1002/adma.202101589.

[17] G.R. Bhimanapati, et al., 2d Boron nitride, Semiconduct. Semimetals (2016) 101–147, https://doi.org/10.1016/bs.semsem.2016.04.004.

[18] Zhiquan Dai, et al., Cold sintering of van der Waals layered compounds, Open Ceram. 12 (2022) 100304, https://doi.org/10.1016/j.oceram.2022.100304.

[19] Selda Nayir, et al., Cold sintering of a covalently bonded MOS2/graphite composite as a high capacity Li–Ion Electrode, ChemNanoMat. 4 (10) (2018) 1088–1094, https://doi.org/10.1002/cnma.201800342.

[20] D.E. Soule, C.W. Nezbeda, Direct basal-plane shear in single-crystal graphite, J. Appl. Phys. 39 (11) (1968) 5122–5139, https://doi.org/10.1063/1.1655933.

[21] Gwan-Hyoung Lee, et al., Electron tunneling through atomically flat and ultrathin hexagonal boron nitride, Appl. Phys. Lett. 99 (24) (2011), https://doi.org/10.1063/1.3662043.

[22] Oleksii Maruzhenko, et al., Improving the thermal and electrical properties of polymer composites by ordered distribution of carbon micro- and nanofillers, Int. J. Heat. Mass Transf. 138 (2019) 75–84, https://doi.org/10.1016/j.ijheatmasstransfer.2019.04.043.

[23] M Oshikiri, et al., Comparison of the electron effective mass of the N-Type ZnO in the wurtzite structure measured by cyclotron resonance and calculated from First Principle Theory, Physica B 298 (1–4) (2001) 472–476, https://doi.org/10.1016/s0921-4526(01)00365-9.

[24] Benjamin Kaufmann, et al., Investigation of schottky barriers at PD-ZnO junctions in varistors, J. Eur. Ceram. Soc. 40 (11) (2020) 3771–3775, https://doi.org/10.1016/j.jeurceramsoc.2020.02.003.

[25] Se-Won Han, et al., The microstructure and conduction mechanism of the nonlinear ZnO Varistor with Al/Sub 2/o/sub 3/additions, in: Proceedings of 5th International Conference on Properties and Applications of Dielectric Materials, 1997, https://doi.org/10.1109/icpadm.1997.616574.

[26] Vinod K.S. Shante, Scott Kirkpatrick, An introduction to percolation theory, Adv. Phys. 20 (85) (1971) 325–357, https://doi.org/10.1080/00018737100101261.